J Mater Sci (2010) 45:4126–4132
DOI 10.1007/s10853-010-4501-9

Dual orientation and variant selection during diffusional transformation of austenite to allotriomorphic ferrite

Dae Woo Kim · Dong-Woo Suh · R. S. Qin · H. K. D. H. Bhadeshia

Received: 23 February 2010 / Accepted: 7 April 2010 / Published online: 27 April 2010

Abstract The crystallographic relationship between austenite and grain boundary nucleated allotriomorphic ferrite has been investigated using electron back-scattered diffraction with a view to establishing a mechanism of variant selection. It is possible in some circumstances for the ferrite to adopt a favoured orientation relationship with both of the austenite grains with which it is in contact. However, the theoretical probability for the development of such a dual orientation has in previous work been shown to be very small, although experiments indicate otherwise. In this work, we have discovered experimentally that the probability of dual orientations is significantly increased when adjacent austenite grains are connected by special high-angle boundaries. Crystallographic calculations validate these observations and lead to the conclusion that simultaneous lattice matching between ferrite and its parent austenite grains is more likely in the presence of certain kinds of microscopic texture in the austenite. The phenomenon of dual orientation provides a criterion for crystallographic variant selection during diffusional transformation.

D. W. Kim · D.-W. Suh
Graduate Institute of Ferrous Technology, POSTECH, Pohang 790-784, Republic of Korea

R. S. Qin
Imperial College London, London SW7 2AZ, UK

H. K. D. H. Bhadeshia (✉)
University of Cambridge, Cambridge CB2 3QZ, UK
e-mail: hkdb@cam.ac.uk

Introduction

The criteria for crystallographic variant selection during a displacive transformation are well-established because there is a pronounced interaction between the transformation strain and an externally imposed system of stresses or strains [4, 5, 10, 12, 17, 20]. The classic Patel and Cohen [20] analysis, which gives the mechanical driving force due to this interaction has been successful in explaining the selection of crystallographic variants in the context of martensitic or bainitic transformations in steels [8, 9, 16, 17].

However, the same does not apply to allotriomorphic ferrite whose formation involves long-range diffusion and which undoubtedly is the dominant phase in the vast majority of steels produced. The term *allotriomorph* implies that the shape of the particle does not respect its internal crystalline symmetry [2]; the ferrite nucleates at an austenite grain boundary and its morphology is determined by the contours of the boundary, which represents an easy diffusion path. It has long been considered that during nucleation, a low-energy orientation relationship develops between the ferrite and one of the austenite grains with which it is in contact, and that this fixes how the ferrite is related to the other austenite grain. The 'low-energy orientation' is often assumed to be close to Kurdjumov–Sachs [18] or Nishiyama–Wasserman [19, 25] , whence densly-packed planes and corresponding close-packed directions from the two lattices are approximately parallel.

Therefore, an allotriomorph (α) will in general adopt a low-energy orientation relationship with one of the austenite grains and a random orientation with the other grain with which it has contact. There is, however, long-standing evidence to suggest that of the 24 ferrite-orientations possible in a given austenite crystal, that which is favoured is the one which is able to simultaneously match with both

the adjacent austenite grains [1, 14, 15, 22]. In contrast, it has been shown by calculation that the probability of simultaneous matching is small even when the parent austenite exhibits macroscopic crystallographic texture [13]. Ferrite, which is able to achieve a low-energy orientation with both austenite grains, is said to exhibit a 'dual orientation', and such simultaneous matching can only occur for some of the 24 possible orientations, then this provides a mechanism for variant selection during phase transformation. Note that there is a certain amount of subjectivity in claiming the existence of dual orientations because of experimental error and because it is necessary first to define an acceptable level of deviation from an ideal low-energy orientation [13].

In the course of some crystallographic investigations, we have discovered another phenomenon which may increase the probability of dual orientations, i.e. when the adjacent austenite grains are oriented in such a way that there is a large proportion of lattice points, which are common to the two grains (coincidence site lattices).

The chemical composition of the experimental alloy used is Fe–0.595C–0.98Si–1.10Mn–1.50Al wt%. It is designed so that a small amount of allotriomorphic ferrite can be generated at a relatively high temperature, followed by isothermal transformation to bainitic ferrite and retained austenite. Nearly 20% of austenite is retained in the final microstructure, permitting its crystallographic orientation to be determined without ambiguity.

The samples geometry is illustrated in Fig. 1; the active region was cylindrical, 5 mm diameter and 10 mm long, for use in a push rod BAHR DIL-805 high speed dilatometer with radio frequency induction heating. The procedure is illustrated in Fig. 1. The sample was first austenitised by heating at 9 °C s^{-1} to 1, 200 °C and holding there for 10 min, followed by cooling to the 740 °C where it was held for 15 min to generate allotriomorphic ferrite; it was then quenched to 450 °C for isothermal transformation into bainitic ferrite for 10 min. The cooling rate during each of the steps was 60 °C s^{-1} to avoid any unintentional phase transformation. The sample was deformed in tension, by 15% uniform elongation prior to the onset of the ferrite transformation, Fig. 1. Note that there is a significant time gap between the end of deformation and the beginning of ferrite formation.

All samples were etched with 2 vol.% nital solution and areas were identified using microhardness indents for further examination in a scanning electron microscope. The surface of the sample is usually deformed during metallographic preparation, so the indented samples were polished using colloidal silica for 3 min. The orientations of allotriomorphic ferrite and austenite were measured using electron back scattered diffraction (EBSD) on a ZEISS SUPRATM scanning electron microscope.

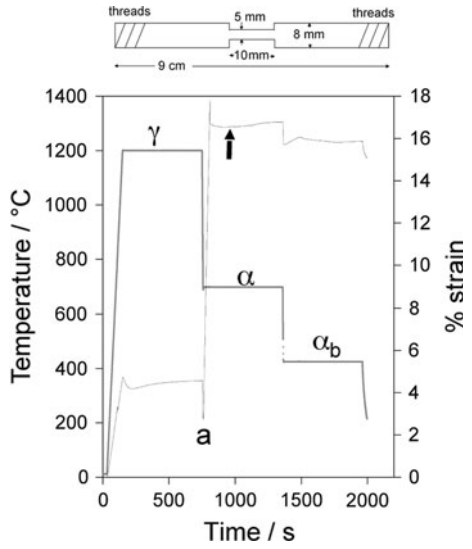

Fig. 1 The thermo-mechanical procedure for the dilatometric experiments. The deformation step was in some cases omitted for comparison purposes. Austenite, allotriomorphic ferrite and bainitic ferrite are represented by the symbols γ, α and α_b, respectively. The point 'a' marks the beginning of the deformation. The *arrow* marks the point where allotriomorphic ferrite begins to form during isothermal holding at 740 °C

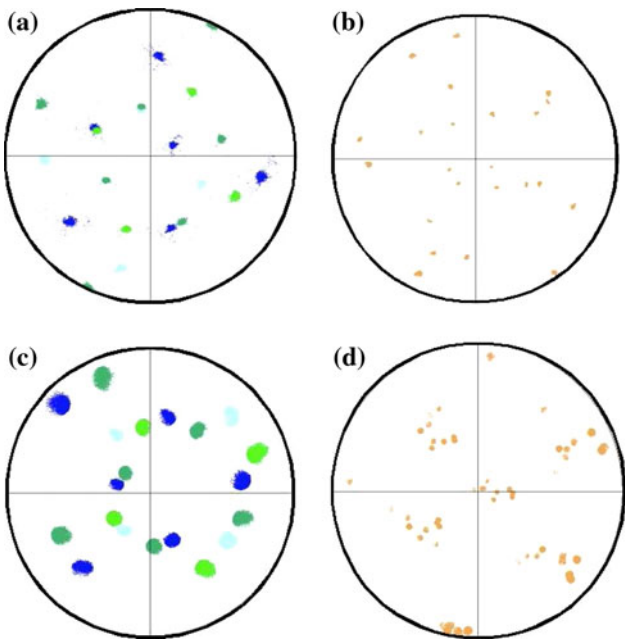

Fig. 2 **a** {110} and {111} poles from two grains of undeformed austenite of the sample illustrated in Fig. 3. **b** Corresponding {110} pole figure of allotriomorphic ferrite that grows from undeformed austenite. **c** {110} and {111} poles from two grains of deformed austenite of the sample illustrated in Fig. 4. The direction of applied strain is vertical. **d** Corresponding {110} pole figure of allotriomorphic ferrite that grows from deformed austenite

It is important to comment on the accuracy of the EBSD observations as applied in the present work so as to avoid over-interpretation of the experimental data. Figure 2

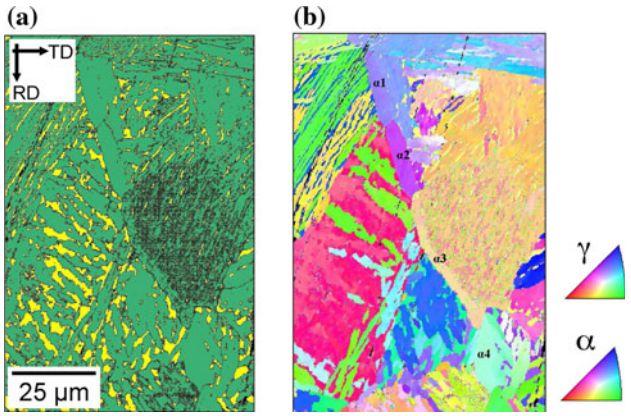

Fig. 3 Transformation in underformed sample. **a** Phase map with *yellow* corresponding to austenite and *green* to allotriomorphic or bainitic ferrite, and **b** inverse pole figure (Color figure online)

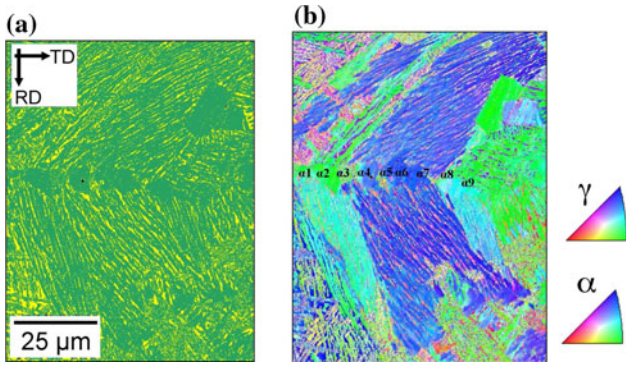

Fig. 4 Transformation in sample deformed to 15% elongation during transformation to allotriomorphic ferrite. **a** Phase map with *yellow* corresponding to austenite and *green* to allotriomorphic or bainitic ferrite, and **b** inverse pole figure (Color figure online)

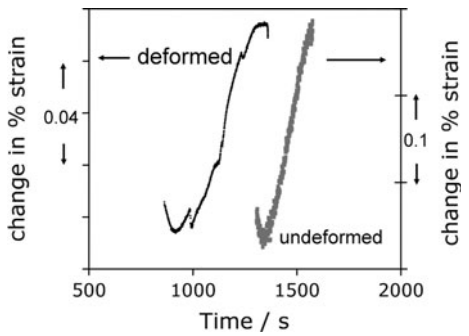

Fig. 5 Comparison of the rate at which allotriomorphic ferrite forms during isothermal transformation in deformed and undeformed austenite

shows three stereograms where for perfect and very large crystals, each pole would effectively be a point. However, the retained austenite is in a finely divided state and that contributes to a broadening of diffracted beams; it also will contain dislocations generated by the formation of bainite [23] which result in strain broadening. Figure 2a shows that the angular spread of the individual poles of austenite is much larger than that of the allotriomorphic ferrite, Fig. 2b, which is expected since the ferrite is relatively coarse and grows by diffusional transformation and hence does not inherit the defect structure of the parent phase. The diffraction from the austenite deteriorates further when it is plastically deformed at 740 °C, as illustrated in Fig. 2c. We estimate that the poles of austenite are in fact spread over about 5° and those of ferrite over <2°. These values indicate the precision of the measurements reported below and any interpretations must be made in this context.

Numerical method

Whereas the Kurdjumov–Sachs and Nishiyama–Wasserman type orientations are frequently quoted as the orientation adopted by allotriomorphic ferrite, the actual observations usually assume that a $\{110\}_\alpha$ plane is exactly parallel to a $\{111\}_\gamma$ plane. However, techniques such as conventional electron diffraction and EBSD do not have sufficient precision to reach this conclusion. The relationship selected here to represent a low-energy orientation is Kurdjumov–Sachs, simply for the pragmatic reason that it represents a more general case with 24 crystallographic variants per austenite grain, whereas the exact Nishiyama–Wasserman relation only results in 12 such variants. Since the actual

Table 1 Deviation from the exact Kurdjumov–Sachs orientation for the ferrite grains illustrated in Fig. 3

Grain	Deviation axis–angle pairs for (γ ΔJ γ)				Σ
	With respect to γ_1		With respect to γ_2		
α_1	[−0.567 −0.659 −0.493]	1.60°	[0.984 0.085 −0.153]	21.98°	–
α_2	[−0.696 0.717 0.014]	4.47°	[−0.034 −0.996 A0.074]	17.01°	–
α_3	[0.087 −0.289 −0.953]	1.34°	[−0.743 0.042 0.667]	20.42°	–
α_4	[0.578 0.531 0.618]	30.43°	[−0.590 0.734 0.331]	2.30°	–
γ_1			[−0.530 0.013 −0.848]	37.2°	–
γ_2	[−0.530 0.013 −0.848]	37.2°			

Table 2 Deviation from the exact Kurdjumov–Sachs orientation for the ferrite grains illustrated in 4

Grain	Deviation axis–angle pairs for (γ ΔJ γ)				Σ
	With respect to γ_1		With respect to γ_2		
α_1	[0.903 −0.221 −0.365]	4.14°	[0.956 −0.289 −0.011]	13.80°	
α_2	[0.560 0.781 −0.272]	10.99°	[−0.699 −0.567 0.434]	5.15°	
α_3	[−0.159 0.985 0.061]	14.60°	[0.016 0.972 −0.230]	4.43°	
α_4	[−0.527 0.821 −0.216]	14.37°	[−0.847 0.289 −0.444]	2.94°	
α_5	[0.6817 −0.726 0.086]	18.98°	[−0.406 −0.898 −0.165]	4.84°	
α_6	[0.863 0.503 0.042]	12.92°	[0.292 0.934 0.202]	4.40°	
α_7	[0.010 −0.744 −0.667]	9.98°	[0.577 −0.096 0.810]	10.09°	
α_8	[−0.369 −0.613 −0.697]	4.34°	[−0.872 0.302 −0.383]	10.39°	
α_9	[0.716 −0.671 0.189]	3.78°	[0.958 0.220 −0.178]	9.57°	
γ_1			[−0.444 0.220 −0.178]	22.4°	–
γ_2	[−0.444 0.220 −0.178]	22.4°			–

orientation relation is likely to be irrational, one must expect 24 variants; the methodology used in this work applies whatever the actual orientation relationship. A specific variant (say number 1) of the Kurdjumov–Sachs orientation can be represented by a rotation matrix[1]:

$$(\alpha\ \mathrm{J}^{1}_{\mathrm{KS}}\ \gamma) = \begin{pmatrix} 0.741582 & -0.666667 & 0.074915 \\ 0.64983 & 0.741582 & -0.166667 \\ 0.166667 & 0.074915 & 0.983163 \end{pmatrix}. \tag{1}$$

The other $i = 2$ to 24 variants can be generated by applying the symmetry operations of the cubic lattice. Suppose that the ith variant of ferrite forms at a grain boundary between two austenite crystals γ_1 and γ_2, the given (γ_1 J^{i}_{KS} α), it follows that

$$(\gamma_2\ \mathrm{J}\ \alpha) = (\gamma_2\ \mathrm{J}\ \gamma_1)(\gamma_1\ \mathrm{J}^{1}_{\mathrm{KS}}\ \alpha) \tag{2}$$

where (γ_1 $\mathrm{J}^{i}_{\mathrm{KS}}$ α) is the inverse of (α $\mathrm{J}^{i}_{\mathrm{KS}}$ γ_1), and (γ_2 J γ_1) describes how the two crystals of austenite are related. In order to determine whether the ferrite simultaneously exhibits a low-energy orientation with both of the austenite grains, it is necessary to determine how close (γ_2 J α) is to a Kurdjumov–Sachs orientation. This can be done by defining a 'difference' matrix as follows:

$$(\gamma\ \Delta\mathrm{J}\ \gamma) = (\gamma\ \mathrm{J}\ \alpha)(\alpha\ \mathrm{J}^{\mathrm{i}}_{\mathrm{KS}}\ \gamma) \qquad \text{for } i = 1 \rightarrow 24. \tag{3}$$

This difference matrix can also be expressed as a right-handed rotation θ about a specific axis of rotation. Because of the symmetry of the cubic system, there are 24 equivalent axis–angle pairs and the one corresponding to the smallest rotation is chosen here to represent the deviation from an exact Kurdjumov–Sachs orientation.

Results and discussion

Figure 3 shows four ferrite grains at an austenite grain boundary. It is clear from the orientation image that each ferrite grain is related only to one of the adjacent austenite grains, and the data presented in Table 1 confirm this. The last column indicates the Σ coincidence site lattice (CSL) number for the austenite grain boundary at which the ferrite nucleates; an absence of a number indicates that the γ/γ orientation does not coincide with a CSL orientation. It is noticeable that the ferrite grains grow as layers along the austenite grain boundaries. One reason for this is a small nucleation rate, which then allows the few grains that form to develop along the austenite grain surfaces and this further limits the number density of ferrite grains. Since the focus of the present work is to look at crystallography, it would be useful to increase the nucleation rate.

Not surprisingly, Fig. 5 shows that the overall rate at which allotriomorphic ferrite forms in a sample, which is deformed prior to transformation, is greater than one in which the ferrite grows from undeformed austenite. It is well known that deformation of the austenite increases the nucleation rate at the austenite grain boundaries [11, 21]. Figure 4 shows that this is indeed achieved when the transformation occurs from deformed austenite, with a relatively large number density of ferrite grains at the austenite grain boundaries. The grains have colours in the orientation image, which are similar to those of the bainite on either side of the grain boundary. Table 2 shows that deviation from the exact Kurdjumov–Sachs orientation is

[1] Throughout this article, we use the vector and matrix notation due to Bowles and MacKenzie which is particularly good at avoiding confusion between frames of reference [3, 6, 7].

significant but small, an indication that each ferrite grain attempts to lattice match with both of the adjacent austenite crystals. Further studies were focused on deformed samples. It is not possible to comment on the generality of this result without extensive observations, but the possibility of such matching must increase when the orientation difference between the adjacent austenite grains is small [13].

It has been pointed out [1] that the small chance of finding a dual orientation relation may be related to the fact allotriomorphic ferrite can grow rapidly into surrounding grains with which it is randomly oriented. However, the greatly increased nucleation rate in deformed austenite confines the ferrite grains by impingement so that the chance of observing dual orientations is greatly increased.

Figure 6 shows a large number of equiaxed ferrite grains, the crystallographic data for which are listed in Table 3, classified into three groups. The interesting feature of the data is that two of the austenite grain boundaries correspond closely to the $\Sigma = 3$ and $\Sigma = 11\gamma/\gamma$ orientation. The former of course corresponds to the highest number density of coincidence points and hence a relatively low interfacial energy per unit area; it is not surprising therefore that there is an absence of ferrite grains at the boundary. The first two groups listed in Table 3 are grains that have nucleated at the $\Sigma = 11$ boundary and it is particularly noticeable that most of these ferrite crystals are able to match fairly well to both of the austenite grains related across the $\Sigma = 11$ grain boundary.

In contrast, the ferrite nucleated at the general boundary between γ_3/γ_6 do not fit well with the dual orientation concept. These observations led us to believe that nucleation at austenite grains related by low Σ values would be worth investigating theoretically to see whether such γ/γ orientations favour the formation of dual orientation ferrite grains.

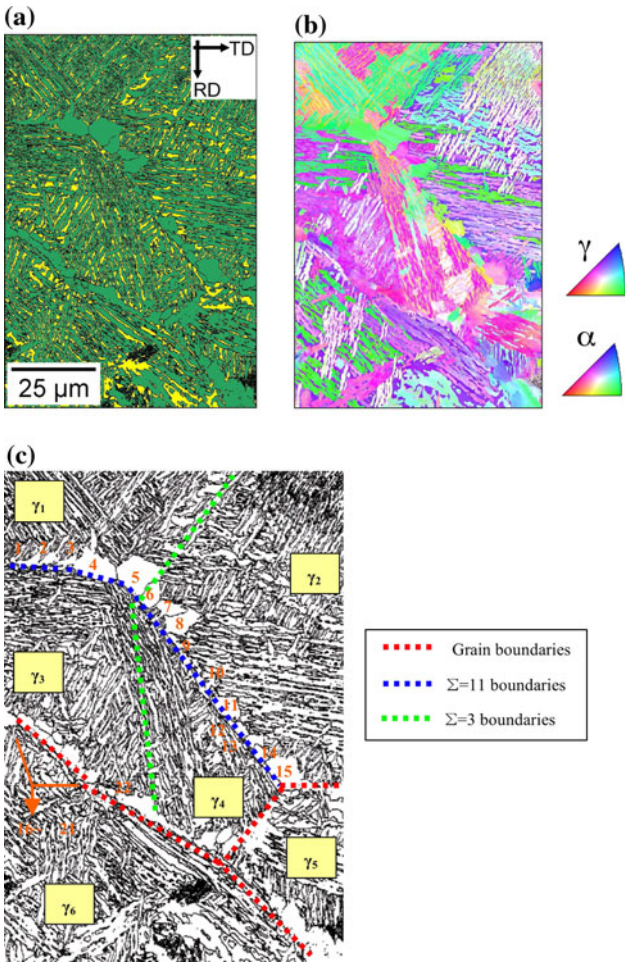

Fig. 6 Transformation in sample deformed to 15% elongation during transformation to allotriomorphic ferrite. **a** Phase map with *yellow* corresponding to austenite and *green* to allotriomorphic or bainitic ferrite, and **b** inverse pole figure. **c** Image quality map (Color figure online)

Calculations

Assuming a specific γ_1/γ_2 orientation relationship defined by an exact Σ value, and ferrite forming with an exact Kurdjumov–Sachs orientation with γ_1, it was possible to assess for all 24 variants of ferrite possible in γ_1 to calculate how far the ferrite grain deviates from the Kurdjumov–Sachs orientation with γ_2. The results are illustrated in Fig. 6 and show clearly that the propensity for developing dual orientations is large for $\Sigma = 11$, even when Δ_{max} is set to a low value.[2]

When larger values of Δ_{max} are permitted in the definition of dual orientations, other Σ boundaries show significant increases in the ability for ferrite to simultaneously match both of the adjacent austenite grains (Table 4). Notice that $\Sigma = 3$ features as the most favoured for the development of dual orientations, but the γ/γ interfacial energy corresponding to this CSL is very low and hence such boundaries are relatively ineffective as heterogeneous nucleation sites for ferrite. What this also emphasises is that any model for the prediction of transformation texture, which is based on the selection of variants, which lead to dual orientations, must at the same time take into account the interfacial energy per unit area of the austenite grain boundaries available in the microstructure.

Finally, it is worth noting that there is considerable activity in a related field, that of *grain boundary engineering*, where efforts are made to introduce a large density of coincidence site boundaries in order to control the properties of steels [24, 26]. If such steels transform to allotriomorphic ferrite, then variant selection should play

[2] Δ_{max} represents the maximum deviation permitted from the exact Kurdjumov–Sachs orientation relationship [13].

Table 3 Deviation from the exact Kurdjumov–Sachs orientation for the ferrite grains illustrated in Fig. 6. Notice that the axis–angle pairs relating γ_1/γ_2 and γ_2/γ_4 correspond quite closely to that expected from $\Sigma = 11$ at a 50.5° about $\langle 0\ 1\ 1 \rangle$ [3]

Grain	Deviation axis–angle pairs for (γ ΔJ γ)				Σ
	With respect to γ_i		With respect to γ_j		
Group 1					
α_1	[0.903 −0.221 −0.365]	4.13°	[0.206 −0.866 0.454]	3.10°	
α_2	[0.843 0.138 −0.519]	4.84°	[0.618 −0.749 0.234]	2.45°	
α_3	[−0.048 −0.989 0.133]	3.96°	[−0.851 0.497 0.165]	4.61°	
α_4	[0.028 −0.713 −0.700]	4.95°	[−0.047 −0.697 −0.714]	6.81°	
α_5	[0.742 −0.334 −0.580]	1.95°	[−0.285 0.925 −0.249]	4.17°	
γ_1			[0.004 0.745 0.667]	47.4°	11
γ_3	[0.004 0.745 0.667]	47.4°			11
Group 2					
α_6	[0.643 0.752 −0.154]	11.16°	[0.507 −0.856 0.097]	30.93°	
α_7	[0.410 −0.911 −0.001]	7.75°	[−0.442 0.680 0.583]	3.42°	
α_8	[−0.112 −0.278 −0.953]	4.60°	[0.319 0.926 −0.197]	5.11°	
α_9	[0.748 0.662 0.032]	5.36°	[0.286 0.306 −0.907]	2.96°	
α_{10}	[−0.450 0.438 −0.777]	5.25°	[−0.259 0.275 −0.925]	17.55°	
α_{11}	[0.917 0.094 0.386]	27.26°	[−0.827 −0.365 0.426]	5.38°	
α_{12}	[−0.908 0.285 0.304]	5.52°	[−0.739 0.656 −0.147]	20.25°	
α_{13}	[−0.300 −0.679 −0.669]	7.27°	[0.935 −0.343 0.084]	9.57°	
α_{14}	[−0.992 0.095 0.073]	5.18°	[−0.752 0.425 0.501]	19.37°	
α_{15}	[0.712 −0.564 0.416]	8.54°	[0.585 0.511 0.629]	10.33°	
γ_2			[−0.059 0.699 −0.713]	50.32°	11
γ_4	[−0.059 0.699 −0.713]	50.32°			11
Group 3					
α_{16}	[0.968 0.205 0.139]	1.57°	[0.824 −0.018 0.565]	24.05°	
α_{17}	[0.097 −0.928 0.359]	12.26°	[−0.292 −0.715 −0.635]	5.58°	
α_{18}	[−0.947 −0.302 −0.101]	25.48°	[−0.850 0.473 −0.229]	3.40°	
α_{19}	[0.988 0.053 −0.138]	22.46°	[−0.634 −0.659 −0.404]	1.76°	
α_{20}	[0.167 0.540 −0.824]	5.21°	[−0.107 −0.986 0.123]	12.40°	
α_{21}	[−0.282 0.835 −0.470]	3.79°	[0.121 −0.991 0.041]	8.04°	
α_{22}	[0.879 −0.240 0.411]	2.91°	[−0.698 0.621 0.354]	13.38°	
α_{23}	[0.032 −0.845 −0.532]	16.31°	[0.476 0.214 −0.852]	4.89°	
γ_3			[0.809 0.498 0.312]	31.2°	–
γ_6	[0.809 0.498 0.312]	31.2°	–		

an exaggerated role in the development of crystallographic texture.

Finally, it is worth pointing out that even when the ferrite has a low-energy orientation relationship with austenite, and it displays the same colour in an orientation image as the bainite, it remains to be proven that these two phases have the same crystallography. This is because an irrational orientation relation is *necessary* in the case of a displacive transformation such as bainite [6, 27], but not necessarily so for diffusional transformations such as allotriomorphic ferrite [2].

Conclusions

In earlier work [13], we demonstrated that the probability of ferrite nucleating with good lattice matching with more than one austenite grain with which it is in contact (dual orientations), is small. This conclusion was not changed significantly by introducing common macroscopically defined crystallographic textures into the austenite (for example, Goss, Cube etc.).

However, the macroscopic texture descriptions of the kind considered do not uniquely reflect the orientations

Table 4 Calculated percentage of dual orientation at austenite grains related by the coincidence site lattice orientation indicated. Δ_{max} represents the maximum deviation permitted from the exact Kurdjumov–Sachs orientation relationship

Σ	Percentage dual orientation			
	$\Delta_{max} = 1°$	$\Delta_{max} = 5°$	$\Delta_{max} = 10°$	$\Delta_{max} = 15°$
3	25	25	50	75
5	0	0	0	0
7	0	0	0	0
9	0	0	16.66	20.83
11	8.33	8.33	16.66	50
13a	0	0	30.33	30.33
13b	0	0	0	0
15	0	0	16.66	20.83
17a	0	0	30.33	30.33
19a	0	0	16.66	16.66
19b	0	12.5	25	50
21a	0	25	29.16	29.16

between adjacent austenite grains as described, for example, by the coincidence site lattice.

It is found in the present work that certain coincidence site lattices favour the development dual orientations. This has been verified both experimentally and theoretically and may explain early work where the probability of observing dual orientations was noted to be significant. It also appears that the chance of observing dual orientations increases when transformation occurs from deformed austenite since the associated high rate of nucleation prevents the spread of allotriomorphic ferrite.

It would be useful in future work to build up a three-dimensional picture of the crystallography, one which includes the indices of the grain boundary plane. This could be done using serial sectioning based on focused ion beam machining [28].

Acknowledgements The authors are grateful to Professor Hae-Geon Lee for the provision of laboratory facilities at GIFT. Professor Bhadeshia is grateful for the support from the World Class University Programme of the National Research Foundation of Korea, Ministry of Education, Science and Technology, project number R32-2008-000-10147-0.

References

1. Babu SS, Bhadeshia HKDH (1991) Mater Sci Eng A 142:209
2. Bhadeshia HKDH (1985) Prog Mater Sci 29:321
3. Bhadeshia HKDH (2001) Geometry of crystals, 2nd edn. Institute of Materials, London
4. Bogers AJ, Burgers WG (1964) Acta Metall 12:255
5. Bokros JC, Parker ER (1963) Acta Metall 11:1291
6. Bowles JS, MacKenzie JK (1954) Acta Metall 2:129
7. Christian JW (2003) Theory of transformations in metal and alloys, part I, 3rd edn. Pergamon Press, Oxford, UK
8. Geijselaers HJM, Perdahcioglu ES (2009) Scr Mater 60:29
9. Perdahcioglu ES, Geijselaers HJM, Groen M (2008) Scr Mater 58:947
10. Higo Y, Lecroisey F, Mori T (1974) Acta Metall 22:313
11. Inagaki H (1986) Z Metallkd 77:36
12. Kato M, Mori T (1976) Acta Metall 24:853
13. Kim DW, Qin RS, Bhadeshia HKDH (2009) Mater Sci Technol 25:892
14. King AD, Bell T (1975) Metall Trans A 6:1419
15. King AD, Bell T (1976) Metallography 9:397
16. Kundu S (2007) Transformation strain and crystallographic texture in steels. PhD thesis, University of Cambridge, Cambridge, UK. http://www.msm.cam.ac.uk/phase-trans/2000/phd.html#kundu,
17. Kundu S, Bhadeshia HKDH (2006) Scr Mater 55:779
18. Kurdjumov GV, Sachs G (1930) Z Phys A 64:325
19. Nishiyama Z (1934) Sci Rep Tohoku Imp Univ 23:637
20. Patel JR, Cohen M (1953) Acta Metall 1:531
21. Speich GR, Cuddy LJ, Gordon CR, DeArdo AJ (1984) In: Marder AR, Goldstein JI (eds) Phase transformations in ferrous alloys. TMS-AIME, Warrendale, PA, p 341
22. Suh DW, Kang JH, Oh KH, Lee HC (2002) Scr Mater 46:375
23. Swallow E, Bhadeshia HKDH (1996) Mater Sci Technol 12:121
24. Tsurekawa S, Okamoto K, Kawahara K, Watanabe T (2005) J Mater Sci 40:895. doi:10.1007/s10853-005-6507-2
25. Wassermann G (1933) Arch Eisenhüttenwes 6:347
26. Watanabe T, Tsurekawa S, Zhao X, Zuo L (2006) Scr Mater 54:969
27. Wechsler MS, Lieberman DS, Read TA (1953) Trans AIME J Met 197:1503
28. West GD, Thomson RC (2009) J Microsc 233:442